Biogeosciences

Discussions

1 # Representing methane emissions from wet tropical forest soils
2 # using microbial functional groups constrained by soil diffusivity

3 Debjani Sihi[1], Xiaofeng Xu[2], Mónica Salazar Ortiz[3], Christine S. O'Connell[4,5], Whendee L.
4 Silver[5], Carla López-Lloreda[6], Julia M. Brenner[1], Ryan K. Quinn[1,7], Jana R. Phillips[1], Brent D.
5 Newman[8], and Melanie A. Mayes[1]*

6 [1]Climate Change Science Institute and Environmental Sciences Division, Oak Ridge National Laboratory, Oak Ridge,
7 TN, 37831, USA
8 [2]Department of Biology, San Diego State University, San Diego, CA, 92182-4614, USA
9 [3]Institute of Plant Science and Microbiology, University of Hamburg, Hamburg, 20148, Germany
10 [4]Department of Environmental Studies, Macalester College, St. Paul, MN, 55105-1899, USA
11 [5]Department of Environmental Science, Policy and Management, University of California, Berkeley, CA, 94720-
12 3114, USA
13 [6]Department of Natural Resources and the Environment, University of New Hampshire, Durham, NH, 03824, USA
14 [7]Department of Biology, Boston University, Boston, MA, 02215, USA
15 [8]Earth and Environmental Sciences Division, Los Alamos National Laboratory, Los Alamos, NM, 87545, USA

16 *Correspondence to*: Melanie A. Mayes (mayesma@ornl.gov)

17 **Abstract.** Tropical ecosystems contribute significantly to global emissions of methane (CH_4) and landscape
18 topography influences the rate of CH_4 emissions from wet tropical forest soils. However, extreme events such as
19 drought can alter normal topographic patterns of emissions. Here we explain the dynamics of CH_4 emissions during
20 normal and drought conditions across a catena in the Luquillo Experimental Forest, Puerto Rico. Valley soils served
21 as the major source of CH_4 emissions in a normal precipitation year (2016), but drought recovery in 2015 resulted in
22 dramatic pulses in CH_4 emissions from all topographic positions. Geochemical parameters including dissolved organic
23 carbon (C) (ridge $\gg$ slope $\gg$ valley), acetate (ridge $\geq$ slope $>$ valley), and soil pH (valley $\gg$ slope $\gg$ ridge), and
24 meteorological parameters like soil moisture (valley $>$ slope $=$ ridge) and oxygen (O_2) concentrations (slope $=$ ridge $>$
25 valley) varied across the catena. During the drought, soil moisture decreased in the slope and ridge and O_2
26 concentrations increased in the valley. We simulated the dynamics of CH_4 emissions with the Microbial Model for
27 Methane Dynamics-Dual Arrhenius and Michaelis Menten (M3D-DAMM) which couples a microbial functional
28 group CH_4 model with a diffusivity module for solute and gas transport within soil microsites. Contrasting patterns of
29 soil moisture, O_2, acetate, and associated changes in soil pH with topography regulated simulated CH_4 emissions, but
30 emissions were also altered by rate-limited diffusion in soil microsites. Changes in simulated available substrate for
31 CH_4 production (acetate, CO_2, and H_2) and oxidation (O_2 and CH_4) increased the predicted biomass of methanotrophs
32 during the drought event and methanogens during drought recovery, which in turn affected net emissions of CH_4. A
33 variance-based sensitivity analysis suggested that parameters related to acetotrophic methanogenesis and
34 methanotrophy were most critical to simulate net CH_4 emissions. This study enhanced the predictive capability for
35 CH_4 emissions associated with complex topography and drought in wet tropical forest soils.

36 **Copyright statement.** This manuscript has been authored by UT-Battelle, LLC, under contract DE-AC05-
37 00OR22725 with the U.S. Department of Energy (DOE). The US government retains and the publisher, by accepting

38 the article for publication, acknowledges that the US government retains a nonexclusive, paid-up, irrevocable,

39 worldwide license to publish or reproduce the published form of this manuscript, or allow others to do so, for US

40 government purposes. DOE will provide public access to these results of federally sponsored research in accordance

41 with the DOE Public Access Plan (http://energy.gov/downloads/doe-public-access-plan).

42 **1 Introduction**

43 Wet tropical forest soils contribute significantly to global emissions of methane (CH_4; Pachauri et al., 2014). Although

44 net emissions of CH_4 from upland soils are infrequent in temperate climates, studies show that CH_4 emissions are

45 common in wet tropical forests (Cattânio et al., 2002; Keller and Matson, 1994; Silver et al., 1999; Teh et al., 2005;

46 Verchot et al., 2000). Landscape topography can strongly influence the proportions of CH_4 production and oxidation

47 in mountainous tropical regions, affecting net emissions (Silver et al., 1999; O'Connell et al., 2018). Climate, and

48 specifically patterns in rainfall, also affect emissions from tropical forests. Climate change may increase the frequency

49 and severity of extreme rainfall and drought events, altering the spatial and temporal dynamics of CH_4 emissions

50 through changes in redox dynamics and substrate availability (Silver et al., 1999; Chadwick et al., 2016; Neelin et al.,

51 2006). Thus, accurately estimating CH_4 emissions under a variety of climatic and topographic conditions is important

52 for predicting soil carbon-climate feedbacks in the humid tropical biome.

53 Several studies have reported the effect of drought events on biogenic CH_4 emissions across different wet tropical

54 forest soils. For example, Aronson et al. (2019) demonstrated that the lower soil moisture conditions during 2015-16

55 El Niño event increased atmospheric consumption of soil CH_4 in a wet tropical forest soil of Costa Rica. Similarly, a

56 large-scale, 5-year throughfall exclusion experiment in a moist tropical forest in Brazil also reported increased

57 consumption of atmospheric CH_4 under the drought treatment, followed by a recovery of CH_4 emissions to pre-

58 treatment values after the experiment ceased (Davidson et al., 2004, 2008). Using rainout shelters, Wood and Silver

59 (2012) found spatial variability in CH_4 oxidation rates, with an increase of 480% uptake in valleys in Puerto Rico.

60 Recently, O'Connell et al. (2018) reported increasing consumption of atmospheric CH_4 during a Caribbean drought

61 event, followed by increased production of CH_4 after the drought was over. The post-drought net CH_4 emission rates

62 were higher than the pre-drought emissions, such that the benefits to atmospheric radiation imparted by the lowered

63 emissions during the drought were eliminated. The sharp differences between pre- and post-drought emissions

64 suggested that drought affected the balance of methanogenesis and methanotrophy in the soils, but the study lacked

65 analysis of the microbial community's contributions to these two separate processes.

66 The concept of "microsites" inside soil aggregates or within soil micropores can help explain the coexistence of

67 oxidative and reductive processes in soils (Silver et al., 1999; Teh and Silver, 2006). Oxygen can remain inside

68 micropores during saturated conditions, and likewise, anoxic conditions can persist in microsites under extended

69 droughts. The observed rapid flush of CH_4 in response to a post-drought wetting event (O'Connell et al., 2018)

70 suggests methanogenesis continued during the drought in soil microsites, despite low soil moisture and high O_2 supply

71 (Andersen et al., 1998; Bosse and Frenzel, 1998; Teh et al., 2005; von Fischer and Hedin, 2002). Finely-textured soils

72 common to the humid tropics can facilitate the co-existence of reduced solute and gas species with O_2 because the rate

73 of solute and gaseous exchanges is controlled by diffusion into and out of microaggregates (Hall and Silver, 2013;

74 Liptzin et al., 2010; Silver et al., 2013).

75 To explain the diverse observations of CH_4 emissions during and after drought across a wet tropical forest catena, we

76 hypothesized that explicit representations of diffusion into microsites for gas and solute transport would be required.

77 To account for the balance of methanotrophy and methanogenesis, separate microbial functional groups for CH_4

78 production and oxidation would need to be defined. Therefore, a microbial functional group model for CH_4 production

79 and consumption (Xu et al., 2015) was merged with a soil diffusivity module (Davidson et al., 2012; Sihi et al., 2018)

80 to simulate the dynamics of net *in situ* CH_4 emissions from soil microsites (Sihi et al., 2020). This module considers

81 three key mechanisms for CH_4 production and consumption: acetoclastic methanogenesis (production from acetate)

82 and hydrogenotrophic methanogenesis (production from H_2 and CO_2), and aerobic methanotrophy (oxidation of CH_4

83 and reduction of O_2) (Fig. 1). Here we report a modeling experiment to explain contrasting patterns of observed CH_4

84 emissions following a severe drought in 2015 and we provide new data to describe CH_4 emissions under non-drought

85 conditions in 2016. We explicitly account for changes in soil moisture, O_2, acetate, and microbial functional group

86 dynamics within soil microsites in the model.

87 **2 Materials and methods**

88 **2.1 Study site**

89 The study was conducted across a wet tropical forest catena near the El Verde Research Station in the Luquillo

90 Experimental Forest in northeastern Puerto Rico in the United States (Latitude 18°19'16.83" N, Longitude

91 65°49'10.13" W). The site is part of a National Science Foundation Long-Term Ecological Research (LTER) and

92 Critical Zone Observatory (CZO) site and is also part of the U.S. Department of Energy's Next Generation Ecosystem

93 Experiment-Tropics. The mean annual temperature at the site is 23 °C and the long-term mean rainfall is ~3500 mm

94 yr$_{-1}$ with low seasonality (Scatena, 1989). Inter-annual variability of rainfall ranges between 2600 mm yr$_{-1}$ to 5800

95 mm yr$_{-1}$, sometimes associated with extreme rainfall events (~100 mm day$_{-1}$) from Caribbean storm systems (Heartsill-

96 Scalley et al., 2007).

97 The landscape at the field site is highly dissected with short catenas, characterized by a land surface distance of < 30

98 m from ridgetop to valley (O'Connell et al., 2018). This study partitioned sampling along a catena from ridgetop,

99 slope, and valley topographic positions (Fig. S1). The soils are clay-rich Ultisols, which were derived from basaltic

100 and andesitic volcanoclastic parent materials. Soils are acidic (average pH is 4.3 and 5.1 in ridge and valley

101 topographic positions, respectively, Fig. 2). The valley soils have ~30% clay and ~15% sand, while the ridge soils

102 have ~22% clay and ~30% sand (Brenner et al., 2019). The soils contain high concentrations of iron (Fe) and aluminum

103 (Al) (oxy)hydroxides where their relative concentrations vary along the catena and differences in Fe speciation are

104 associated with variable redox conditions (Hall and Silver, 2013, 2015). The forest composition is relatively diverse

105 with the mature Tabonuco (*Dacryodes excelsa* Vahl) and Sierra palm (*Prestoea montana*) trees being most dominant

106 (Scatena and Lugo, 1995; Wadsworth et al., 1951).

2.2 Soil and porewater sampling

To initialize the model, soil samples were collected quarterly from the ridgetop, slope, and valley positions from 0-10 cm depth. The soil pH was determined using a 1:2 ratio of soil:solution using a glass electrode with 0.005 M $CaCl_2$ as the equilibrated soil solution (Thomas, 1996; Sihi et al. 2020b). Porewater samples were collected approximately weekly using macro-rhizon soil water samplers (Rhizosphere Research Products B.V.; Wageningen, The Netherlands) installed at 10- and 30-cm depths in the ridge, slope, and valley topographic positions (Sihi et al., 2020c). The soil water samples were analyzed for organic acid concentrations (acetate) using High Performance Liquid Chromatography (Dionex ICS-5000+ Thermo-Fisher Waltham, MA, USA) with the Dionex IonPac AS11-HC column using a potassium hydroxide eluent and gradient elution. The samples were analyzed for total dissolved organic carbon (DOC) using a Shimadzu total organic C analyzer (Shimadzu TOC-L CSH/CSN Analyzer Baltimore, MD, USA). The soil and porewater measurements were conducted in 2017-2018 (the number of samples *n* ranged between 20 to 35, Fig. 2) to initialize different model parameters for the catena, because measurements were not available for 2015-2016. To that end, the chemical data were used as the reference characteristics of the bulk soil, and the temporal evolution of DOC, acetate, and soil pH at the microsites were calculated using probability distributions of soil moisture and O_2 across soil microsites over the two-year measurement window. Soil bulk density and particle density values were taken from O'Connell et al. (2018).

2.3 In situ methane flux and soil driver measurements

Campbell Scientific CS 655 soil moisture and temperature sensors and Apogee SO-110 O_2 sensors were co-located with soil gas flux chambers at 15 cm soil depth along the catena, each with five replications along five transects (Fig. S1) (O'Connell et al. 2018). Following Liptzin et al. (2011), soil O_2 sensors were installed in gas-permeable soil equilibration chambers (295 cm_3). Data from these sensors were collected hourly using Campbell Scientific CR10000 data loggers and AM16/32B multiplexers (Campbell Scientific, Logan, UT, USA), which were processed using site-based calibration equations.

Soil CH_4 emissions along the catena were measured during 2015 (February 26 to December 23, O'Connell et al. 2018; Silver, 2018) and 2016 (April 5 to July 18) (Sihi et al., 2020d) using a Cavity Ring-Down Spectroscopy gas analyzer (Picarro G2508, Santa Clara, CA, USA) connected to 12 automated eosAC closed dynamic soil chambers (Pumpanen et al., 2004) using a multiplexer (Eosense Inc., Dartmouth, Nova Scotia, Canada). Data for soil CH_4 emissions were processed using eosAnalyze-AC (v3.5.0) software followed by a series of quality control protocols (O'Connell et al. 2018). We used daily average values of drivers (soil temperature, soil moisture, and O_2 concentrations) and CH_4 emissions in the modeling exercise. See O'Connell et al (2018) for more information on the soil sensor, chamber arrays, and the data analysis pipeline.

The data from the 2015 Caribbean drought was partitioned into four distinct periods (O'Connell et al., 2018): (1) pre-drought from day of year (DOY) 57 to 115 (dark gray on Fig. 3), (2) the drought from DOY 116 to 236 (medium gray on Fig. 3), (3) drought recovery from DOY 237 to 328 (light gray on Fig. 3), and (4) post-drought from DOY 329 to 354 (white on Fig. 3). Total precipitation during the drought period was 700 mm in 2015 and 1088 mm during the

Biogeosciences

Discussions

Open Access

142 same time frame in 2016 (Meteorological data from El Verde Field Station: NADP Tower, available at

143 https://luq.lter.network/data/luqmetadata127).

144 **2.4 Modelling approach**

145 **2.4.1 Microbial functional group model for methane production and oxidation**

146 An existing microbial functional group-based model for CH_4 production and consumption (Xu et al., 2015) was

147 adapted for this research (Sihi, 2020). As shown in Fig. 1, acetate and H_2/CO_2 represent substrate [$Substrate_{func_i}$]

148 (nmole cm^{-3}) for acetotrophic and hydrogenotrophic methanogenesis reactions, respectively. On the other hand, CH_4

149 and O_2 concentrations represent substrate for the methanotrophy reaction. The overall reaction rates are represented

150 as:

151 $Reaction_{rate_i} = Biomass_{func_i} \times \frac{GrowR_{func_i}}{Efficiency_{func_i}} \times \frac{[Substrate_{func_{1...n}}]}{[Substrate_{func_{1...n}}] + KM_{func_{1...n}}} \times f(T) \times f(pH)$ (1)

152 where $Reaction_{rate_i}$ (in nmole cm^{-3} hr^{-1}) is rate of CH_4 production and/or consumption under variable substrate

153 concentrations. $Biomass_{func_i}$ (nmole cm^{-3}) represents microbial functional groups: acetoclastic methanogens,

154 hydrogenotrophic methanogens, and aerobic methanotrophs, respectively. Growth rates and substrate use efficiencies

155 of microbial functional groups are represented as $GrowR_{func_i}$ (hr^{-1}) and $Efficiency_{func_i}$ (unitless), respectively (Table

156 1). The substrate limitation on CH_4 production is imposed by assuming a Michaelis-Menten relationship between the

157 substrates and the half-saturation constants for CH_4 production and oxidation, $KM_{func_{1...n}}$ (nmole cm^{-3}). Although

158 minor contributions of iron dependent anaerobic CH_4 oxidation to net CH_4 emissions can be expected in our study site

159 (Ettwig et al., 2016), we did not represent this process here.

160 The extent of change in $Biomass_{func_i}$ ($dBiomass_{func_i}$) is controlled by the balance between $Growth_{func_i}$ and

161 $Death_{func_i}$ following:

162 $\frac{dBiomass_{func_i}}{dt_{func_i}} = Growth_{func_i} - Death_{func_i}$ (2)

163 $Growth_{func} = Efficiency_{func_i} \times Reaction_{rate_i}$ (3)

164 where $Growth_{func_i}$ is calculated as a multiplicative function of $Efficiency_{func_i}$ and the $Reaction_{rate_i}$.

165 $Death_{func_i} = DeadR_{func_i} \times Biomass_{func_i}$ (4)

166 and $Death_{func_i}$ is a function of $DeadR_{func_i}$ (death rate, Table 1) and $Biomass_{func_i}$ (microbial biomass).

167 All rate equations were modified by the scalers for temperature, f(T) and pH, f(pH) functions, described below. We

168 represented the temperature effect, f(T), using a classic Q_{10} function:

169 $f(T) = Q_{10_i}^{\frac{Temperature_{soil} - Temperature_{reference}}{10}}$ (5)

170 We represented the pH effect, f(pH), based on Cao et al (1995):

171 $f(pH) = \frac{(pH - pH_{minimum}) * (pH - pH_{maximum})}{(pH - pH_{minimum}) * (pH - pH_{maximum}) - (pH - pH_{optimum})^2}$ (6)

172 where we set the minimum, optimum, and maximum soil pH values to 4, 7, and 10, respectively. Following Xu et al.

173 (2015), we considered the contribution of acetate to pH as follows:

174 $$\text{pH} = -1 * \log(10^{\text{pH}_{\text{initial}}} + 4.2\text{E} - 9 * \text{Acetate})$$ (7)

175 Although other mechanisms to alter soil pH are present at the site, e.g., Fe reduction and oxidation (Teh et al., 2005;

176 Hall and Silver, 2013), these are not considered in the model at this time. Calibrated values of $\text{GrowR}_{\text{func}_i}$,

177 $\text{DeadR}_{\text{func}_i}$, $\text{Efficiency}_{\text{func}_i}$, $\text{KM}_{\text{func}_i}$, and Q_{10_i} are presented in Table 1.

178 **2.4.2 Diffusion module for gaseous and solute transport in soil profile and across soil-air boundary**

179 In order to account for the diffusion of gases across the soil-air boundary and solutes (e.g. acetate) through soil water

180 films (Fig. 1), we added the diffusion module of the Dual Arrhenius and Michaelis Menten (DAMM) model (Davidson

181 et al., 2012; Sihi, 2020; Sihi et al., 2018, 2020a) to the existing microbial functional group model, which we refer to

182 as M3D-DAMM. We calculated initial concentration of gases like O_2, H_2, CO_2, and CH_4, $[\text{Gas}_{\text{conc}}]$, (unit: V V$_{-1}$), as a

183 function of a unitless diffusion coefficient of gas in air (D_{gas}), volume fraction of gas in air (V V$_{-1}$), and gas diffusivity

184 ($a^{4/3}$) as follows:

185 $$[\text{Gas}_{\text{conc}}] = D_{\text{gas}} \times \text{atmospheric concentration} \times a^{4/3}$$ (8)

186 where $a^{4/3}$ represents the tortuosity of diffusion pathway for gases as a function of soil water (SoilM) and temperature

187 (SoilT):

188 $$a^{4/3} = \left(\text{Porosity} - \frac{\text{SoilM}}{100}\right)^{4/3} \times \left(\frac{\text{SoilT}+273.15}{293.15}\right)^{1.75}$$ (9)

189 where the air-filled porosity (a) was calculated by subtracting the volume fraction of soil moisture (V V$_{-1}$) from total

190 porosity. Porosity was calculated as:

191 $$(1 - \frac{\text{Bulk density}}{\text{Particle density}})$$ (10)

192 The exponent of 4/3 accounts for diffusivity of gases through porous media (Davidson and Trumbore., 1995). The

193 exponent of 1.75 represents the temperature response of gaseous diffusion (Massman, 1998; Davidson et al., 2006).

194 Following Davidson et al. (2012), the value used for gaseous diffusivity coefficient (D_{gas}) was calculated based on an

195 assumed boundary condition such that the concentration of gaseous substrates in the soil pore space would be

196 equivalent to the volume fraction of gases in air under completely dry conditions.

197 We assumed another boundary condition to determine the value of the aqueous diffusion coefficient, D_{liq}, such that

198 soluble substrates like acetate would be available at the enzymatic reaction site under conditions with saturating soil

199 water content (Davidson et al., 2012):

200 $$D_{\text{liq}} = \frac{1}{\text{Porosity}^3}$$ (11)

201 We represented soluble substrates (acetate) diffused through a soil water film as Aqueous $-$ substrate (μmole L$_{-1}$),

202 which we calculated as follows:

203 $$\text{Aqueous} - \text{substrate}_{\text{av}} = \text{Aqueous} - \text{substrate} \times D_{\text{liq}} \times (\frac{\text{SoilM}}{100})^3$$ (12)

204 where the $(\frac{\text{SoilM}}{100})^3$ term represents the diffusion rate of aqueous substrates to the enzymatic active site (Papendick and

205 Campbell, 1981). Concentrations of acetate in the aqueous phase (μmole L$_{-1}$) were obtained from the measurements

206 across the catena averaged by depths (10 and 30 cm) of rhizon samplers.

207   We calculated CH$_4$ emissions, CH$_{4emission}$ (unit: µmole m^{-2} hr^{-1}), as a function of concentration ($[CH_{4conc}]$),

208   production (CH$_{4prod}$), and oxidation (CH$_{4ox}$) of CH$_4$, multiplied by the equivalent "depth" (set to 15 cm) (for cm^{-3}

209   volume to cm^{-2} area conversion) and 10$_4$ (for m$_2$ to cm$_2$ conversion) as follows:

210   $$CH_{4emission} = [CH_{4conc}] + (CH_{4prod} - CH_{4ox}) \times 10^4 \times depth \qquad (13)$$

211   We simulated production, consumption, and diffusion processes within soil microsites using a log-normal probability

212   distribution function of soil moisture and available C (Fig. 1). The average values of individual processes across

213   simulated microsites (represented by "i") represent the reaction in the bulk soil, which we constrained using the net

214   measured CH$_4$ emissions (detailed information and equations on microsite probability distribution function can be

215   found in Sihi et al., 2020a).

216   $$Bulk\ soil_{average} = \frac{\sum Frequency_i \times [microsite]_i}{Total\ microsites} \qquad (14)$$

217   We directly adapted the probability distribution function of soil moisture and C from Sihi et al. (2020a), which

218   constrained values of Frequency$_i$ of soil microsites. We also set the number of total microsites to 10,000, which

219   represents the envelope of simulated microsites in Sihi et al. (2020a).

220   2.4.3 Sensitivity Analysis

221   We evaluated the sensitivity of model parameters with a global variance-based sensitivity analysis using the *R-*

222   *multisensi* package. This method uses a global sensitivity index ($0 < GSI < 1$) to determine the sensitivity of CH$_4$

223   emissions to model parameter values (Bidot et al., 2018). To that end, parameters with high GSI values may explain

224   high temporal variations of the observed CH$_4$ emissions and those with low GSI values are insignificant to reproduce

225   the temporal dynamics of CH$_4$ emissions.

226   2.4.4 Statistical Analysis

227   We used R (version 3.5.1) for statistical analyses, modeling, and visualization purposes (R Core Team, 2018).

228   Statistical analyses and figures were produced using *R-ggstatsplot* (Patil, 2018) and *R-ggplot2* (Wickham, 2016)

229   packages. Differences in soil and porewater chemistry across the catena were compared using robust t-test.

230   Correlograms for soil temperature, soil moisture, O$_2$, and soil CH$_4$ emissions were created using adjusted Holm

231   correlation coefficients. All statistical analyses were conducted at the 5% significance level. We implemented the

232   M3D-DAMM model using *R-FME* package (Soetaert, 2016).

233   3 Results

234   3.1 Observational dynamics of soil biogeochemistry

235   Soil and porewater chemistry varied along the catena (Fig. 2). Dissolved organic carbon (DOC) values followed the

236   trend of ridge >> slope >> valley ($p \leq 0.001$). Soil DOC concentrations (mean ± SE) were 0.55 ± 0.10, 0.30 ± 0.03,

237   and 0.18 ± 0.03 mg g^{-1} in ridge, slope, and valley soils, respectively. Organic acid (acetate) concentrations were

238   significantly higher in the ridge (6.57 ± 1.48 µmole L^{-1}) and slope (6.42 ± 2.19 µmole L^{-1}) than in the valley ($1.80 \pm$

239   0.20 µmole L-1) (p = 0.003). Soil pH followed the trend of valley >> slope >> ridge (p < 0.001). Average soil pH
240   ranged from 4.25 ± 0.11 in the ridge, to 4.49 ± 0.08 in the slope, and to 5.05 ± 0.09 in the valley.

241   Soil moisture and soil O_2 concentrations were distinctly different in the drought year (2015) compared to 2016. The
242   drought in 2015 decreased soil moisture in the slope and ridge soils and increased O_2 concentrations in the valley soils
243   (Fig. 3) (also see O'Connell et al., 2018). Generally, average soil moisture was higher in the valley (0.47 ± 0.05 in
244   2015 and 0.51 ± 0.01 v v-1 in 2016) as compared to the ridge (0.31 ± 0.12 in 2015 and 0.39 ± 0.03 v v-1 in 2016) and
245   slope (0.30 ± 0.16 in 2015 and 0.41 ± 0.04 v v-1 in 2016). Average O_2 concentrations were generally lower in the
246   valley (11.54 ± 5.94 in 2015 and 6.30 ± 2.96 % in 2016) as compared to the ridge (18.37 ± 0.72 in 2015 and $17.52 \pm$
247   0.42 % in 2016) and slope (18.09 ± 1.22 in 2015 and 16.89 ± 0.58 % in 2016). After the drought ended, the recovery
248   of soil moisture in the ridge and slope soils proceeded more quickly than the recovery of O_2 concentrations in the
249   valley soils (Fig. 3). Soil temperature ranges were averaged across the topographic gradient and were similar in both
250   years (average was 21.58 ± 1.88 in 2015 and 22.97 ± 1.04 °C in 2016).

251   In 2016, net CH_4 emissions were generally positive in the valley and were marginally negative in the ridge and slope
252   (Fig. 4). The dynamics of CH_4 were very different following the 2015 drought, resulting in net positive CH_4 emissions
253   in the post-drought period for all topographic positions (Fig. 3) (as described in more detail in O'Connell et al. 2018).
254   The magnitude of CH_4 emissions was greater in the valley, followed by the slope and then the ridge.

255   The strength of the relationships between net CH_4 emissions and soil temperature, moisture, and O_2 concentrations
256   were contingent on both topographic position and year (2015 vs 2016) (Fig. 5). For example, the relation between
257   CH_4 emissions and soil moisture was stronger in 2016 (normal year) than in 2015 (drought year). The correlation
258   between CH_4 emissions and O_2 concentrations was stronger and more negative in 2016 than 2015. Correlations
259   between soil moisture and O_2 concentrations were negative and stronger in 2016. Correlation coefficients between
260   soil O_2 concentrations and CH_4 emissions were negative and strongest for valley soils and lowest for ridge soils in
261   2015, but were uncorrelated in 2016 for ridge and slope soils (Fig. S2).

262   **3.2 Model simulations of methanogenesis and methanotrophy**

263   In general, there was little bias in the relationships between the observed and simulated CH_4 emissions (Fig. 6). The
264   model explained 72% and 67% of the variation in soil CH_4 emissions for 2015 and 2016, respectively, although the
265   model performance varied across the catena (Figs. 6, S3, S4). Overall, simulated CH_4 emissions captured the trend of
266   valley >> slope ≥ ridge for 2016. The model also captured the dramatically different dynamics of field CH_4 emissions
267   as a function of topography during and after the 2015 drought. Net positive CH_4 emissions were simulated in the
268   drought recovery and post-drought periods in the ridge and slope in 2015, while net negative emissions were simulated
269   in the other times for these landscape positions. Additionally, simulated net CH_4 emissions were decreased during the
270   drought and drought recovery in the valley soils, as well as the strong net CH_4 emissions in the valley soils in the post-
271   drought period.

272   The ridge and slope positions were more similar to each other than to the valley soils. Simulated biomass of
273   acetoclastic methanogens and hydrogenotrophic methanogens decreased strongly, resulting in decreased production
274   of acetate and hydrogen during the 2015 drought in the ridge and slope positions (Figs. S5, S6). Gross CH_4 production

275 therefore decreased during these time periods (Fig. S7). Simultaneously, as soil moisture decreased, simulated
276 methanotrophic biomass increased during the drought (Fig. S5). The simulated biomass of both acetoclastic
277 methanogens and hydrogenotrophic methanogens increased dramatically in the ridge and slope soils during drought
278 recovery (acetoclastic methanogens: 3.3 and 5.3 times higher than drought period for ridge and slope, respectively;
279 hydrogenotrophic methanogens: 6.1 and 12 times higher than drought period for ridge and slope, respectively) and
280 post-drought (acetoclastic methanogens: 5.2 and 8.8 times higher than drought period for ridge and slope, respectively;
281 hydrogenotrophic methanogens: 12 and 24 times higher than drought period for ridge and slope, respectively) period.
282 Concomitantly, production of acetate and H_2 was much higher in the ridge and slope soils during the drought recovery
283 (acetate: 1.8 and 2.4 times than drought period for ridge and slope soils, respectively; H_2: 3.5 and 6.0 times than
284 drought period for ridge and slope soils, respectively) and the post-drought (acetate: 2.3 and 3.2 times than drought
285 period for ridge and slope, respectively; H_2: 5.6 and 10 times than drought period for ridge and slope, respectively)
286 period. Together, gross CH_4 production in the ridge and slope soils was significantly higher during the drought
287 recovery (1.9 and 2.5 times than drought period for ridge and slope, respectively) and post-drought periods (3.4 and
288 4.6 times than drought period for ridge and slope, respectively) compared to the drought (Fig. S7). Simulated
289 production of acetate was increased that also lowered soil pH values during drought recovery (Fig. S6), with a more
290 pronounced effect in the ridge and slope soils. Additionally, simulated methanotrophic biomass and CH_4 oxidation
291 decreased during the post-drought period (Figs. S5, S7), which is the same time period during which net CH_4
292 production increased strongly.

293 For the valley soils, simulated values of acetoclastic methanogens and concomitant acetate production increased
294 during the 2015 drought (Figs. S5, S6). During the drought recovery and post-drought period, both acetoclastic
295 methanogens and acetate production decreased in the valley, while hydrogenotrophic methanogens and H_2 production
296 were stable. Gross CH_4 production, however, remained relatively flat during the drought event in the valley, and only
297 increased during the post-drought period (Fig. S7). Simulated CH_4 oxidation and methanotrophic biomass, on the
298 other hand, increased dramatically during the drought and drought recovery period (Figs. S5, S7), and then decreased
299 strongly during the post-drought period. However, simulated methanotrophic biomass was smaller in the valley soils
300 compared to the ridge and slope soils. Methane oxidation by methanotrophs exerted strong controls on simulated net
301 CH_4 emissions, not only in the valley but in all the topographic positions.

302 **3.3 The influence of microsites on net methane emissions**

303 Concomitant with decreased soil moisture, the simulated diffusion of gases (O_2, H_2) was enhanced during the drought
304 event in 2015, while diffusion of the solute (acetate) was dramatically decreased, particularly for the ridge and slope
305 soils (Fig. S8). However, reduction in soil moisture can inhibit fermentative hydrogen production (Cabrol et al., 2017).
306 Consequently, simulated gross CH_4 production through hydrogenotrophic and acetoclastic pathways both decreased
307 during the drought event for the ridge and slope positions (Figs. S7, S9). As soil moisture increased during the drought
308 recovery and post-drought periods, the diffusion of gases decreased, and diffusion of acetate increased in the ridge
309 and slope soils (Fig. S8). Consequently, simulated values of gross CH_4 production increased and gross CH_4 oxidation

310   decreased during drought recovery and the post-drought period (Fig. S7). These factors likely contribute to the large

311   pulses of net CH_4 emissions during the post-drought period for ridge and slope positions (Fig. 3).

312   Overall, the valley soils were relatively insensitive to changes in the rate of diffusion of either gases or solutes (Fig.

313   S8), most likely because soil moisture remained relatively stable, regardless of drought conditions (Fig. 3). The lower

314   sand and higher clay contents in the valley soils (Brenner et al. 2019), as well as the lower topographic position, likely

315   caused the valley soils to remain wetter than the slope and ridge soils. Therefore, simulated values of gross CH_4

316   production were fairly stable in the valley soils (Fig. S7) during the drought and drought recovery period.

317   Simulated production, oxidation, and net flux of CH_4 was further modified by reactions occurring within soil

318   microsites. For example, during the drought (~DOY 200 in 2015), gross CH_4 production was more frequent in soil

319   microsites in the valley compared to the slope and ridge (Fig. 7). Simulated values of CH_4 oxidation were much greater

320   in microsites in the slope and ridge positions, so the net CH_4 emissions were positive in the valley soils and negative

321   in the ridge and slope positions. During the 2015 post-drought period (DOY 345), the frequency of CH_4 production

322   was much greater in all topographic positions compared to pre-drought period (DOY 200), and it was also more

323   enhanced in the valley soils compared to the slope and ridge. Thus, net positive CH_4 emissions were observed in all

324   topographic positions in the post-drought period (Fig. 3). Methane oxidation at DOY 345 was much greater in the

325   ridge and slope compared to the valley, similar to predictions at DOY 200. Therefore, the prominent CH_4 emissions

326   from all three topographic positions were primarily due to increased production (CH_4 production on DOY 345 was

327   150, 248, and 80 % higher than DOY 200 in ridge, slope, and valley, respectively) rather than decreased oxidation

328   (CH_4 oxidation was 32, 31, and 43 % lower on DOY 345 than DOY 200 in ridge, slope, and valley, respectively),

329   which agrees with previous studies in our site (Teh et al., 2005, 2008; von Fischer and Hedin, 2002)

330   Diffusion into microsites strongly affected the concentrations of gases and solutes experienced by microbes, and

331   differences as a function of topographic position were again predicted. Acetate production and diffusion were

332   enhanced in valley soils during the drought, when compared to the slope and ridge soils (Fig. S10). The H_2 production

333   was also enhanced in the valley soils during the drought, but the wetter valley soils experienced lower rates of H_2

334   diffusion compared to the ridge and slope soils. Increases in O_2 diffusion were also apparent in the ridge and slope

335   soils during the drought, and those increases were greater than in the valley soils. During the post-drought period,

336   however, the frequency of H_2 and O_2 diffusion was much greater for the ridge soils compared to the valley soils (Fig.

337   S10).

338   Of all parameters, the most sensitive ones were those that controlled CH_4 production through the acetoclastic pathway,

339   followed by the parameters related to CH_4 oxidation (Fig. 8). The GSI values for parameters related to acetoclastic

340   methanogenesis and methanotrophy ranged between 0.25 - 0.75, whereas the corresponding GSI values for

341   hydrogenotrophic methanogenesis were always < 0.1.

342   **4 Discussion**

343   **4.1 Mechanisms governing net methane emissions**

344   Although the initial concentrations of available C for fermentation (i.e. DOC) and substrate for acetoclastic

345   methanogenesis (i.e. acetate) in the bulk soil followed the trend of ridge > slope > valley (Fig. 2), the pattern of net

346   CH$_4$ emissions across the catena was opposite (valley >> slope ≥ ridge), especially in 2016 (Fig. 4). The seemingly

347   counterintuitive relations of substrate concentrations in the bulk soil versus net CH$_4$ emissions can be explained by

348   modeling the differing redox conditions across soil microsites. Diffusion promoted the availability of the acetate

349   substrate through more connected soil water films in the wetter valley soils and caused higher gross CH$_4$ production

350   in 2016, as compared to the relatively drier slope and ridge soils (Figs. S7, S8). In contrast, diffusion of gaseous

351   methanotrophic substrates (CH$_4$ and O$_2$) was promoted in the air-filled pore spaces in the drier ridge and slope soils

352   (Fig. S8), resulting in reduced net CH$_4$ emissions for these two topographic positions in 2016 (Fig. 4). Further, reduced

353   diffusion of O$_2$ in the wetter valley soils decreased gross methanotrophy compared to the slope and ridge soils (Figs.

354   S7, S8). Consequently, in 2016, net CH$_4$ emissions dominated the valley soils but were minimal in the ridge and slope

355   soils.

356   On the other hand, the drought event in 2015 decreased the simulated CH$_4$ emission in the slope and ridge soils by

357   decreasing H$_2$ production, and both production (Fig. S6) and diffusion of acetate (Fig. S8). The drought increased the

358   CH$_4$ sink strength of both ridge and slope soils as the observed net CH$_4$ emissions became more negative during the

359   drought compared to the pre-drought period (Fig. 3). Contributing factors predicted by the model include enhanced

360   O$_2$ diffusion into the drier ridge and valley soils (Fig. S8), as well as enhanced methanotrophic biomass (Fig. S5). In

361   the valley, the primary impact of the drought appeared to be due to increased methanotrophy (Fig. S7), since acetate,

362   H$_2$, and gross CH$_4$ production were predicted to continue unabated (Fig. S6, S7). This suggests that drought enhanced

363   consumption of atmospheric CH$_4$ in our site, which is consistent with findings from natural droughts and throughfall

364   exclusion experiments in other wet tropical forest soils (Aronson et al., 2019; Davidson et al., 2004, 2008; Wood and

365   Silver, 2012).

366   However, simulation of observed CH$_4$ emission during drought recovery in 2015 required explicit representations of

367   the complex interaction of the diffusive supply of solute and gases, dynamics of the microbial functional groups, and

368   the associated acetate-pH feedback loop across the distribution of soil microsites (Fig. 3). The drought recovery

369   increased soil moisture which likely prompted anaerobiosis across all topographic locations by significantly reducing

370   gas diffusivity in a fraction of the simulated microsites (11, 17, and 21 % in ridge, slope, and valley, respectively)

371   (McNicol and Silver, 2014; Sihi et al., 2020a; Teh et al., 2005). The return to dominantly reducing conditions also

372   were predicted to stimulate fermentation and the production of acetate (Fig. S6). Enhanced production and diffusion

373   of acetate during recovery (Fig. S8) triggered growth in the predicted biomass of acetoclastic methanogens (Fig. S5),

374   which in turn, increased rates of acetoclastic methanogenesis (Fig. S9).

375   Additionally, acetate is a source of proton and should reduce soil pH (Amaral et al., 1998; Conrad and Klose, 1999;

376   Jones et al., 2003). Previous studies (Xu et al., 2015; Xu et al., 2010) demonstrated that acetate-driven soil pH

377   reduction can reduce net CH$_4$ production by as much as 30%, especially in systems with low initial soil pH like our

378   study site. Given that optimal pH for biological activities peaks near neutral pH, the relatively higher soil pH in the

379   valley versus ridge and slope soil further enhanced the topographic patterns of CH$_4$ emissions (Conrad et al., 1996;

380   also see Figs. 2, 3, and 4). Note that the initial soil pH across the landscape was already in the acidic range (Fig. 2),

381   consequently, the simulated acetate production and concomitant decrease in soil pH during the 2015 drought recovery

382   further suppressed gross CH$_4$ production in ridge soils in comparison to the valley soils (Figs. S6 and S7). Iron

383 reducing bacteria can also suppress CH$_4$ production either by competing with acetoclastic methanogens for acetate
384 substrate or controlling the flow of acetate to both hydrogenotrophic and acetoclastic methanogens by dissimilatory
385 iron reduction (Teh et al., 2008). Additionally, Fe reduction can increase soil pH either by proton consumption and
386 colloid dispersion, while Fe oxidation can lead to more acidic conditions (Hall and Silver, 2013; Thompson et al.,
387 2006). None of these mechanisms are currently represented in the M3D-DAMM model.

388 Although secondary to acetoclastic methanogenesis, simulated rates of hydrogenotrophic methanogenesis also
389 increased in anaerobic microsites (Figs. S9, S10), mediated by increased production of H$_2$ and subsequent stimulation
390 of the biomass of hydrogenotrophic methanogens during the drought recovery in 2015 (Fig. S5). Overall, the absolute
391 values of simulated gross CH$_4$ production through hydrogenotrophic and acetoclastic pathways (Fig. S9) outweighed
392 the simulated gross CH$_4$ oxidation rates (Fig. S7), resulting in net soil CH$_4$ emissions across the catena during the
393 post-drought period (Fig. 3).

394 Hence, high temporal resolution field-scale measurements of CH$_4$ emissions and soil and porewater chemistry
395 facilitated evaluation of the combined effects of soil redox conditions (moisture and O$_2$ concentrations) and associated
396 pH feedbacks on underlying processes occurring across soil microsites, while accounting for variation along the catena
397 as a result of changing climatic drivers over time. The M3D-DAMM model captured the Birch-type effect by
398 quantifying the pulses in soil CH$_4$ emissions as a function of increases in soil moisture following a strong drought
399 (Birch, 1958). Specifically, the model coupled with microsite diffusivity explained CH$_4$ emissions common to wet
400 valley soils and rare in comparatively drier ridge and slope soils and predicted the net release of CH$_4$ emissions from
401 all topographic positions following a strong drought.

4.2 Sensitivity analysis

403 The variance-based sensitivity analysis confirmed the importance of microbial functional groups and their complex
404 interactions with the surrounding biophysical and chemical environments in controlling CH$_4$ production and oxidation.
405 For example, the growth and death of acetoclastic methanogens and the relative efficiency of acetoclastic
406 methanogenesis were the most sensitive parameters (Fig. 8), which is consistent with another modeling effort on CH$_4$
407 fluxes across the Arctic landscape (Wang et al., 2019). Although from completely different ecosystem types, Wang et
408 al. (2019) and the present study confirmed the importance of simulating soil topographies and microbial mechanisms
409 when evaluating the heterogeneities in CH$_4$ fluxes. Representations of both direct (methanogenic substrate) and
410 indirect (soil pH feedback) effects of acetate may have contributed to higher GSI values for parameters representing
411 acetoclastic methanogenesis, which is similar to a previous study (Xu et al., 2015). The sensitivity of CH$_4$ emissions
412 to the parameters representing methanotrophy were secondary to those representing acetoclastic methanogenesis,
413 which is consistent with the increase in methanotrophic biomass during the drought.

4.3 Other processes

415 We did not completely reproduce the net emissions of soil CH$_4$ during the 2015 post-drought period across the catena
416 with the M3D-DAMM model. To capture the full potential of net emissions of CH$_4$ (white shading in Fig. 3) from
417 sesquioxide-rich soils, future modeling efforts may need to explicitly include the dynamics of redox-sensitive elements

418   such as Fe and associated pH feedback under contrasting redox conditions (Barcellos et al., 2018; Bhattacharyya et

419   al., 2018; Hall and Silver, 2013, 2015; O'Connell et al., 2018; Parfitt et al., 1975; and Silver et al., 1999). Wetting

420   events can lower soil redox potential and reduce electron acceptors like Fe(III) to Fe(II). This concomitant reduction

421   of Fe may increase soil pH, especially in anaerobic microsites, which could further increase net emissions of soil CH_4

422   (Tang et al., 2016; Zheng et al., 2019). Accounting for these effects may allow model simulations to better match the

423   highest observed net CH_4 emissions in the post-drought period (Fig. 3).

424   Additionally, the reduction of Fe(III) to Fe(II) has supported anaerobic CH_4 oxidation in other ecosystems (Ettwig et

425   al., 2016). Within this context, a measurable amount of anaerobic oxidation of CH_4 has previously been reported at

426   our study site (Blazewicz et al., 2012). Additionally, Fe-reducing microorganisms can utilize acetate as a substrate

427   and thereby compete with methanogens and reduce net methane emissions (Teh et al., 2008). Given the gradient of

428   Fe in our study site, it is likely that biogeochemical cycling of Fe and CH_4 are coupled (O'Connell et al., 2018) which

429   should be accounted for in future modeling efforts. For example, a modeling study supported the importance of Fe in

430   simulating CH_4 cycling in an Arctic soil (Tang et al., 2016). To that end, building a comprehensive framework that

431   also includes Fe biogeochemistry will afford greater confidence in projected CH_4 emissions from wet tropical forests

432   under future climatic conditions (Bonan et al., 2008; Pachauri et al., 2014; Xu et al., 2016).

433   **5 Conclusions**

434   High-frequency CH_4 emission measurements coupled with real-time soil chemical measurements identified spatial

435   and temporal variations affecting CH_4 production and oxidation in wet tropical forest soils of Puerto Rico. Overall,

436   contrasting patterns of soil moisture between ridge and valley soils played an instrumental role in governing net CH_4

437   emissions. For example, consistently greater soil moisture likely favored methanogenesis by lowering the availability

438   of O_2 in valley soils compared to ridgetop soils, especially in microsites with high soil moisture and soil C content.

439   However, soil porewater chemistry, particularly the concentrations of acetate and associated soil pH influenced the

440   pattern of net emissions of CH_4 across the catena (valley > slope > ridge) during wetting after the 2015 drought. Thus,

441   our results provide compelling evidence of the importance of both hot spots and hot moments in generating and

442   mediating CH_4 emissions in wet tropical forest soils. A microbial functional group-based model coupled with a

443   diffusivity module and consideration of soil microsites adequately reproduced both the spatial and temporal dynamics

444   of soil CH_4 emissions, although mechanisms involving Fe biogeochemistry were neglected.

445   This study suggests that representing the microbial mechanisms and the interactions of microbial functional groups

446   with the soil biophysical and chemical environment across soil microsites is critical for modeling CH_4 production and

447   consumption. To that end, explicit consideration of these underlying mechanisms improved predictions of CH_4

448   dynamics in response to regional climatic events and provided insight into differential dynamics of solute and gas

449   diffusion, different microbial functions, and gross CH_4 production and oxidation as a function of topography. Hence,

450   we contribute to the ongoing development and improvements of Earth system and process models to better simulate

451   microbial roles in CH_4 cycling at regional and global scales. However, observational data concerning the activities of

452   different soil microbial functional groups is still needed to confirm the mechanisms proposed here. Future studies

453   should integrate geochemical and microbiological information relevant for oscillatory redox conditions in wet tropical

454 forests, especially those related to the redox-sensitive elements to build a comprehensive framework for modeling

455 tropical soil CH_4 emissions.

456 **Code and data availability**

457 Meteorological data (http://criticalzone.org/luquillo/data/dataset/4723/) are available from the Luquillo CZO

458 repository. 2015 greenhouse gas fluxes (DOI: 10.6073/pasta/316b68dd254e353e1acfb16d92bac2dc) are available

459 from the Luquillo LTER repository. The 2016 greenhouse gas fluxes (DOI: 10.15485/1632882), soil chemistry (DOI:

460 10.15485/1618870), and rhizon lysimeter data (DOI: 10.15485/1618869) are available from ESS-DIVE repository. R

461 scripts used for this modeling exercise are archived at the following Zenodo repository (DOI:

462 10.5281/zenodo.3890562).

463 **Author contributions**

464 DS performed the data curation of 2016 flux data and the soil and lysimeter data, collated diffusion and microsite

465 processes into the model presented herein, interpreted and validated the model application, developed the

466 visualization, and wrote the original draft. XX provided the model code used in the investigation and assisted with its

467 modification and application. MSO collected the 2016 field flux data. CSO and WLS provided the 2015 flux data and

468 the 2015-2016 field soil measurements for temperature, oxygen, and moisture. CSO developed workflow for field flux

469 data management, cleaning and analysis. WLS acquired the funding, administered the project, and supervised the

470 research team involved with collection of the 2015 data. CLL collected the rhizon water samples and soil samples

471 from the field site, with assistance from MAM. JMB analyzed the rhizon water samples in the lab. JRP, RKQ, and

472 JMB completed the laboratory soil analyses. BDN supplied, installed, and maintained the rhizon water samplers.

473 MAM acquired the funding and administered the project that collected the 2016 data, conceptualized the paper and

474 proposed the methods, supervised the research team, and contributed to the writing, interpretation, and visualization

475 of subsequent drafts. All authors contributed to the manuscript through reviewing and editing subsequent drafts.

476 **Competing interests**

477 The authors declare that they have no conflicts of interest.

478 **Acknowledgements**

491   **References**

492   Amaral, J. A., Ren, T., and Knowles, R.: Atmospheric methane consumption by forest soils and extracted bacteria at

493   different pH values, Appl. Environ. Microbiol., 64, 2397-2402, 1998.

494   Andersen, B. L., Bidoglio, G., Leip, A., and Rembges, D.: A new method to study simultaneous methane oxidation

495   and methane production in soils, Global Biogeochem. Cy., 12, 587-594, https://doi.org/10.1029/98GB01975, 1998.

496   Aronson, E. L., Dierick, D., Botthoff, J., Oberbauer, S., Zelikova, T. J., Harmon, T. C., Rundel, P., Johnson, R. F.,

497   Swanson, A. C., and Pinto-Tomás, A. A.: ENSO-influenced drought drives methane flux dynamics in a tropical wet

498   forest soil, J. Geophys. Res.-Biogeo., 124, 2267-2276, https://doi.org/10.1029/2018JG004832, 2019.

499   Barcellos, D., O'Connell, C. S., Silver, W., Meile, C., and Thompson, A.: Hot spots and hot moments of soil moisture

500   explain fluctuations in iron and carbon cycling in a humid tropical forest soil, Soil Systems, 2, 59,

501   https://doi.org/10.3390/soilsystems2040059, 2018.

502   Bhattacharyya, A., Campbell, A. N., Tfaily, M. M., Lin, Y., Kukkadapu, R. K., Silver, W. L., Nico, P. S., and Pett-

503   Ridge, J.: Redox fluctuations control the coupled cycling of iron and carbon in tropical forest soils, Environ. Sci.

504   Technol., 52, 14129-14139, https://doi.org/10.1021/acs.est.8b03408, 2018.

505   Bidot, C., Monod, H., and Taupin, M.-L.: A quick guide to multisensi, an R package for multivariate sensitivity

506   analyses,   [Available   at   https://mran.microsoft.com/snapshot/2017-08-

507   06/web/packages/multisensi/vignettes/multisensi-vignette.pdf.], 2018.

508   Birch, H.: The effect of soil drying on humus decomposition and nitrogen availability, Plant Soil, 10, 9-31, 1958.

509   Blazewicz, S. J., Petersen, D. G., Waldrop, M. P., and Firestone, M. K.: Anaerobic oxidation of methane in tropical

510   and boreal soils: ecological significance in terrestrial methane cycling, J. Geophys. Res.-Biogeo., 117,

511   https://doi.org/10.1029/2011JG001864, 2012.

512   Bonan, G. B.: Forests and climate change: forcings, feedbacks, and the climate benefits of forests, Science, 320, 1444-

513   1449, 10.1126/science.1155121, 2008.

514   Bosse, U., and Frenzel, P.: Methane emissions from rice microcosms: the balance of production, accumulation and

515   oxidation, Biogeochemistry, 41, 199-214, 1998.

516   Brenner, J., Porter, W., Phillips, J. R., Childs, J., Yang, X., and Mayes, M. A.: Phosphorus sorption on tropical soils

517   with relevance to Earth system model needs, Soil Res., 57, 17-27, https://doi.org/10.1071/SR18197, 2019.

518   Cabrol, L., Marone, A., Tapia-Venegas, E., Steyer, J. P., Ruiz-Filippi, G., and Trably, E.: Microbial ecology of

519   fermentative hydrogen producing bioprocesses: useful insights for driving the ecosystem function. FEMS microbiol.

520   Rev., 41, 158-181, https://doi.org/10.1093/femsre/fuw043, 2017.

521   Cao, M., Dent, J., and Heal, O.: Modeling methane emissions from rice paddies, Global Biogeochem. Cy., 9, 183-

522   195, https://doi.org/10.1029/94GB03231, 1995.

523 Cattânio, J. H., Davidson, E. A., Nepstad, D. C., Verchot, L. V., and Ackerman, I. L.: Unexpected results of a pilot
524 throughfall exclusion experiment on soil emissions of CO2, CH4, N2O, and NO in eastern Amazonia, Biol. Fert. Soils,
525 36, 102-108, 10.1007/s00374-002-0517-x, 2002.

526 Chadwick, R., Good, P., Martin, G., and Rowell, D. P.: Large rainfall changes consistently projected over substantial
527 areas of tropical land, Nat. Clim. Change, 6, 177-181, 10.1038/NCLIMATE2805, 2016.

528 Conrad, R.: Soil microorganisms as controllers of atmospheric trace gases (H2, CO, CH4, OCS, N2O, and NO),
529 Microbiol. Mol. Biol. Rev., 60, 609-640, 1996.

530 Conrad, R., and Klose, M.: Anaerobic conversion of carbon dioxide to methane, acetate and propionate on washed
531 rice roots, FEMS Microbiol. Ecol., 30, 147-155, https://doi.org/10.1111/j.1574-6941.1999.tb00643.x, 1999.

532 Davidson, E. A., Ishida, F. Y., and Nepstad, D. C.: Effects of an experimental drought on soil emissions of carbon
533 dioxide, methane, nitrous oxide, and nitric oxide in a moist tropical forest, Glob. Change Biol., 10, 718-730,
534 https://doi.org/10.1111/j.1365-2486.2004.00762.x, 2004.

535 Davidson, E. A., Nepstad, D. C., Ishida, F. Y., and Brando, P. M.: Effects of an experimental drought and recovery
536 on soil emissions of carbon dioxide, methane, nitrous oxide, and nitric oxide in a moist tropical forest, Glob. Change
537 Biol., 14, 2582-2590, https://doi.org/10.1111/j.1365-2486.2008.01694.x, 2008.

538 Davidson, E. A., Samanta, S., Caramori, S. S., and Savage, K.: The Dual Arrhenius and Michaelis–Menten kinetics
539 model for decomposition of soil organic matter at hourly to seasonal time scales, Glob. Change Biol., 18, 371-384,
540 https://doi.org/10.1111/j.1365-2486.2011.02546.x, 2012.

541 Davidson, E. A., Savage, K. E., Trumbore, S. E., and Borken, W.: Vertical partitioning of CO_2 production within a
542 temperate forest soil, Glob. Change Biol., 12, 944-956, https://doi.org/10.1111/j.1365-2486.2005.01142.x, 2006.

543 Davidson, E. A., and Trumbore, S. E.: Gas diffusivity and production of CO_2 in deep soils of the eastern Amazon,
544 Tellus B: Chem. Phys. Meteorol., 47, 550-565, https://doi.org/10.3402/tellusb.v47i5.16071, 1995.

545 Ettwig, K. F., Zhu, B., Speth, D., Keltjens, J. T., Jetten, M. S., and Kartal, B.: Archaea catalyze iron-dependent
546 anaerobic oxidation of methane, P. Natl. A. Sci., 113, 12792-12796, https://doi.org/10.1073/pnas.1609534113, 2016.

547 Hall, S. J., and Silver, W. L.: Iron oxidation stimulates organic matter decomposition in humid tropical forest soils,
548 Glob. Change Biol., 19, 2804-2813, https://doi.org/10.1111/gcb.12229, 2013.

549 Hall, S. J., and Silver, W. L.: Reducing conditions, reactive metals, and their interactions can explain spatial patterns
550 of surface soil carbon in a humid tropical forest, Biogeochemistry, 125, 149-165, 10.1007/s10533-015-0120-5, 2015.

551 Heartsill-Scalley, T., Scatena, F. N., Estrada, C., McDowell, W., and Lugo, A. E.: Disturbance and long-term patterns
552 of rainfall and throughfall nutrient fluxes in a subtropical wet forest in Puerto Rico, J Hydrol., 333, 472-485,
553 https://doi.org/10.1016/j.jhydrol.2006.09.019, 2007.

554 Jones, D., Dennis, P., Owen, A., and Van Hees, P.: Organic acid behavior in soils–misconceptions and knowledge
555 gaps, Plant Soil, 248, 31-41, 2003.

556 Keller, M., and Matson, P. A.: Biosphere-atmosphere exchange of trace gases in the tropics: Evaluating the effects of
557 land use changes, in: Global Atmospheric-Biospheric Chemistry, Springer, 103-117, 10.1007/978-1-4615-2524-0,
558 1994.

559 Liptzin, D., Silver, W. L., and Detto, M.: Temporal dynamics in soil oxygen and greenhouse gases in two humid
560 tropical forests, Ecosystems, 14, 171-182, 10.1007/s10021-010-9402-x, 2011.

561 Marshall, T.: Gas diffusion in porous media, Science, 130, 100-102, 10.1126/science.130.3367.100-a, 1959.

562 Massman, W.: A review of the molecular diffusivities of H_2O, CO_2, CH_4, CO, O_3, SO_2, NH_3, N_2O, NO, and NO_2 in
563 air, O_2 and N_2 near STP, Atmos. Environ., 32, 1111-1127, https://doi.org/10.1016/S1352-2310(97)00391-9, 1998.

564 McNicol, G., and Silver, W. L.: Separate effects of flooding and anaerobiosis on soil greenhouse gas emissions and
565 redox sensitive biogeochemistry, J. Geophys. Res.-Biogeo., 119, 557-566, https://doi.org/10.1002/2013JG002433,
566 2014.

567 Neelin, J. D., Münnich, M., Su, H., Meyerson, J. E., and Holloway, C. E.: Tropical drying trends in global warming
568 models and observations, P. Natl. A. Sci., 103, 6110-6115, https://doi.org/10.1073/pnas.0601798103, 2006.

569 O'Connell, C. S., Ruan, L., and Silver, W. L.: Drought drives rapid shifts in tropical rainforest soil biogeochemistry
570 and greenhouse gas emissions. Nat. Commun., 9, 1-9, 10.1038/s41467-018-03352-3, 2018.

571 Ostertag, R., Scatena, F. N., and Silver, W. L.: Forest floor decomposition following hurricane litter inputs in several
572 Puerto Rican forests, Ecosystems, 261-273, 10.1007/s10021-002-0203-8, 2003.

573 Pachauri, R. K., Allen, M. R., Barros, V. R., Broome, J., Cramer, W., Christ, R., Church, J. A., Clarke, L., Dahe, Q.,
574 and Dasgupta, P.: Climate change 2014: Synthesis report. Contribution of Working Groups I, II and III to the Fifth
575 Assessment Report of the Intergovernmental Panel on Climate Change, IPCC, 10013/epic.45156.d001, 2014.

576 Papendick, R., and Campbell, G. S.: Theory and measurement of water potential, Water potential relations in soil
577 microbiology, 9, 1-22, https://doi.org/10.2136/sssaspecpub9.c1, 1981.

578 Parfitt, R. L., Atkinson, R. J., and Smart, R. S. C.: The mechanism of phosphate fixation by iron oxides, Soil Sci. Soc.
579 Am. J., 39, 837-841, https://doi.org/10.2136/sssaj1975.03615995003900050017x, 1975.

580 Patil, I.: ggstatsplot: "ggplot2" Based Plots with Statistical Details, [Available at https://CRAN.R-
581 project.org/package=ggstatsplot>], http://doi.org/10.5281/zenodo.2074621, 2018.

582 Pumpanen, J., Kolari, P., Ilvesniemi, H., Minkkinen, K., Vesala, T., Niinistö, S., Lohila, A., Larmola, T., Morero, M.,
583 and Pihlatie, M.: Comparison of different chamber techniques for measuring soil CO_2 efflux, Agr. Forest Meteorol.,
584 123, 159-176, https://doi.org/10.1016/j.agrformet.2003.12.001, 2004.

585 R Core Team.: R: A language and environment for statistical computing, Vienna, Austria, [Available at https://www.r-
586 project.org/], 2018.

587 Scatena, F. N.: An introduction to the physiography and history of the Bisley Experimental Watersheds in the Luquillo
588 Mountains of Puerto Rico, Gen. Tech. Rep. SO-72. New Orleans, LA: US Dept of Agriculture, Forest Service,
589 Southern Forest Experiment Station. 22 p., 72, 1989.

590 Scatena, F., and Lugo, A. E.: Geomorphology, disturbance, and the soil and vegetation of two subtropical wet
591 steepland watersheds of Puerto Rico, Geomorphology, 13, 199-213, https://doi.org/10.1016/0169-555X(95)00021-V,
592 1995.

593 Sihi, D.: PR-model v1.0., 10.5281/zenodo.3890562, [available at
594 https://zenodo.org/record/3890562#.XuOP3DpKg2w], 2020.

595 Sihi, D., Davidson, E. A., Chen, M., Savage, K. E., Richardson, A. D., Keenan, T. F., and Hollinger, D. Y.: Merging
596 a mechanistic enzymatic model of soil heterotrophic respiration into an ecosystem model in two AmeriFlux sites of
597 northeastern USA, Agr. Forest Meteorol., 252, 155-166, https://doi.org/10.1016/j.agrformet.2018.01.026, 2018.

598 Sihi, D., Davidson, E. A., Savage, K. E., and Liang, D.: Simultaneous numerical representation of soil microsite
599 production and consumption of carbon dioxide, methane, and nitrous oxide using probability distribution functions,
600 Glob. Change Biol., 26, 200-218, https://doi.org/10.1111/gcb.14855, 2020a.

601 Sihi, D., López-Lloreda, C., Brenner J. M., Quinn R. K., Phillips J. R., Mayes, M. A.: Soil chemistry data across a
602 catena in the Luquillo Experimental Forest, Puerto Rico, A Comprehensive Framework for Modeling Emissions from
603 Tropical Soils and Wetlands, doi:10.15485/1618870, 2020b.

604 Sihi, D., López-Lloreda, C. Brenner J. M., Quinn R. K., Phillips J. R., Newman B. D., Mayes, M. A.: Porewater data
605 across a catena in the Luquillo Experimental Forest, Puerto Rico. A Comprehensive Framework for Modeling
606 Emissions from Tropical Soils and Wetlands, doi:10.15485/1618869, 2020c.

607 Sihi, D., Salazar-Ortiz, M., Mayes, M. A.: Soil chamber fluxes (CO2 and CH4) across a catena in the Luquillo
608 Experimental Forest, Puerto Rico, A Comprehensive Framework for Modeling Emissions from Tropical Soils and
609 Wetlands, doi:10.15485/1632882, 2020d.

610 Silver, W. L., Liptzin, D., and Almaraz, M.: Soil redox dynamics and biogeochemistry along a tropical elevation
611 gradient, in: Ecological gradient analyses in a tropical landscape, edited by: González, G., Willig, M. R., and Waide,
612 R. B., Ecol. Bull., Wiley-Blackwell, Hoboken, NJ, 54, 195-210, 2013.

613 Silver, W. L., Lugo, A., and Keller, M.: Soil oxygen availability and biogeochemistry along rainfall and topographic
614 gradients in upland wet tropical forest soils, Biogeochemistry, 44, 301-328, 1999.

615 Soetaert, K.: R Package FME: Inverse modelling, sensitivity, Monte Carlo—Applied to a dynamic simulation model,
616 (CRAN Vignette 2). [Available at https://cran. r-project. org/web/packages/FME/vignettes/FMEdyna. pdf.], 2016.

617 Tang, G., Zheng, J., Xu, X., Yang, Z., Graham, D. E., Gu, B., Painter, S. L., and Thornton, P. E.: Biogeochemical
618 modeling of CO_2 and CH_4 production in anoxic Arctic soil microcosms, Biogeosciences, 13, 5021,
619 https://doi.org/10.5194/bg-13-5021-2016, 2016.

620 Teh, Y. A., Dubinsky, E. A., Silver, W. L., and Carlson, C. M.: Suppression of methanogenesis by dissimilatory Fe
621 (III)-reducing bacteria in tropical rain forest soils: Implications for ecosystem methane flux, Glob. Change Biol., 14,
622 413-422, https://doi.org/10.1111/j.1365-2486.2007.01487.x, 2008.

623 Teh, Y. A., and Silver, W. L.: Effects of soil structure destruction on methane production and carbon partitioning
624 between methanogenic pathways in tropical rain forest soils, J. Geophys. Res.-Biogeo., 111,
625 https://doi.org/10.1029/2005JG000020, 2006.

626 Teh, Y. A., Silver, W. L., and Conrad, M. E.: Oxygen effects on methane production and oxidation in humid tropical
627 forest soils, Glob. Change Biol., 11, 1283-1297, https://doi.org/10.1111/j.1365-2486.2005.00983.x, 2005.

628 Thomas, G. W.: Soil pH and soil acidity, Methods of Soil Analysis: Part 3 Chemical Methods, 5, 475-490,
629 https://doi.org/10.2136/sssabookser5.3.c16, 1996.

630 Thompson, A., Chadwick, O. A., Boman, S., and Chorover, J.: Colloid mobilization during soil iron redox oscillations,
631 Environ. Sci. Technol., 40, 5743-5749, https://doi.org/10.1021/es061203b, 2006.

632   Verchot, L. V., Davidson, E. A., Cattânio, J. H., and Ackerman, I. L.: Land-use change and biogeochemical controls
633   of methane fluxes in soils of eastern Amazonia, Ecosystems, 3, 41-56, https://doi.org/10.1007/s100210000009, 2000.
634   Von Fischer, J. C., and Hedin, L. O.: Separating methane production and consumption with a field-based isotope pool
635   dilution technique, Global Biogeochem. Cy., 16, 1034, https://doi.org/10.1029/2001GB001448, 2002.
636   Wadsworth, F. H.: Forest management in the Luquillo mountains, I-setting, Caribbean Forester, 12, 114–124, 1951.
637   Wang, Y., Yuan, F., Yuan, F., Gu, B., Hahn, M. S., Torn, M. S., Ricciuto, D. M., Kumar, J., He, L., Zona, D., Lipson,
638   D. L., Wagner, R., Oechel, W. C., Wullschleger, S. D., Thornton, P. E., and Xu, X.: Mechanistic modeling of
639   microtopographic impact on CH_4 processes in an Alaskan tundra ecosystem using the CLM-Microbe model, J. Adv.
640   Model. Earth Sy., 11, 4228-4304, 2019.
641   Wickham, H.: ggplot2: elegant graphics for data analysis, Springer-Verlag, New York, 2016.
642   Wood, T. E., and Silver, W. L.: Strong spatial variability in trace gas dynamics following experimental drought in a
643   humid tropical forest, Global Biogeochem. Cy., 26, https://doi.org/10.1029/2010GB004014, 2012.
644   Xu, X., Elias, D. A., Graham, D. E., Phelps, T. J., Carroll, S. L., Wullschleger, S. D., and Thornton, P. E.: A microbial
645   functional group-based module for simulating methane production and consumption: Application to an incubated
646   permafrost soil, J. Geophys. Res.-Biogeo., 120, 1315-1333, 10.1002/2015jg002935, 2015.
647   Xu, X. F., Tian, H. Q., Zhang, C., Liu, M. L., Ren, W., Chen, G. S., Lu, C. Q., and Bruhwiler, L.: Attribution of spatial
648   and temporal variations in terrestrial methane flux over North America, Biogeosciences, 7, 3637-3655, 10.5194/bg-
649   7-3637-2010, 2010.
650   Xu, X., Yuan, F., Hanson, P. J., Wullschleger, S. D., Thornton, P. E., Riley, W. J., Song, X., Graham, D. E., Song, C.,
651   and Tian, H.: Reviews and syntheses: Four decades of modeling methane cycling in terrestrial ecosystems,
652   Biogeosciences, 13, 3735-3755, 10.5194/bg-13-3735-2016, 2016.
653   Zheng, J., Thornton, P. E., Painter, S. L., Gu, B., Wullschleger, S. D., and Graham, D. E.: Modeling anaerobic soil
654   organic carbon decomposition in Arctic polygon tundra: insights into soil geochemical influences on carbon
655   mineralization, Biogeosciences, 16, 663-680, 10.5194/bg-16-663-2019, 2019.
656
657
658

659   **Table 1: Fitted values of M3D-DAMM model parameters.**

Parameters	Fitted values	Description	Unit	Source
$GrowR_{H2Methanogens}$	0.31		1/day	Servais et al., 1985
$GrowR_{AceMethanogens}$	1.59	Growth rates	1/day	Servais et al., 1985
$GrowR_{Methanotrophs}$	0.12		1/day	Servais et al., 1985
$DeadR_{H2Methanogens}$	0.03		1/day	Servais et al., 1985
$DeadR_{AceMethanogens}$	0.54	Death rates	1/day	Servais et al., 1985
$DeadR_{Methanotrophs}$	0.008		1/day	Servais et al., 1985
$Efficiency_{H2Methanogens}$	0.2	Substrate	unitless	Grant, 1998
$Efficiency_{AceMethanogens}$	0.04	use	unitless	Kettunen et al., 2003
$Efficiency_{Methanotrophs}$	0.4	efficiencies	unitless	Kettunen et al., 2003
KM_{Ace}	16		mmol/m3	Grant, 1998; McGill et al., 1981
$KM_{H2ProdAce}$	11		µmol/m3	Conrad, 1989
$KM_{H2ProdCH4}$	$2.14*10^{-5}$	Half-saturation	mmol/m3	Fennell and Gossett, 1998
$KM_{CO2ProdCH4}$	$9.08*10^{-9}$	constants	mmol/m3	Stoichiometry theory
$KM_{CH4ProdAce}$	13		mmol/m3	Kettunen et al., 2003
$KM_{CH4ProdO2}$	0.03		mmol/m3	Kettunen et al., 2003
$KM_{CH4OxidCH4}$	0.06		mmol/l	Kettunen et al., 2003
$KM_{CH4OxidO2}$	0.74		mmol/l	Kettunen et al., 2003
$ACmax_{AceProd}$	0.52	Maximum	mmol/m3/h	Smith and Mah, 1966
$Acemax_{H2Prod}$	1.31	reaction rates	mmol acetate/g/h	Conrad, 1989
$rCH4Prod$	0.84	Rate	mol CH_4/mol acetate	Kettunen et al., 2003
$rCH4Oxid$	3.06	constants	mol O_2/mol CH_4	Kettunen et al., 2003
$Q_{10ACMin}$	1.16		unitless	Segers, 1998
$Q_{10AceProd}$	1.21		unitless	Atlas and Bartha, 1987; Kettunen, 2003; Van Hulzen et al., 1999
$Q_{10H2CH4Prod}$	1.27	Temperature	unitless	Segers, 1998
$Q_{10CH4Prod}$	1.13	sensitivities	unitless	Kettunen et al., 2003
$Q_{10CH4Oxid}$	1.18		unitless	Kettunen et al., 2003

660

661   Initial values of model parameters were collected from literature ("Source"). Also see Xu et al. (2015) for detailed information on
662   model parameters.

663
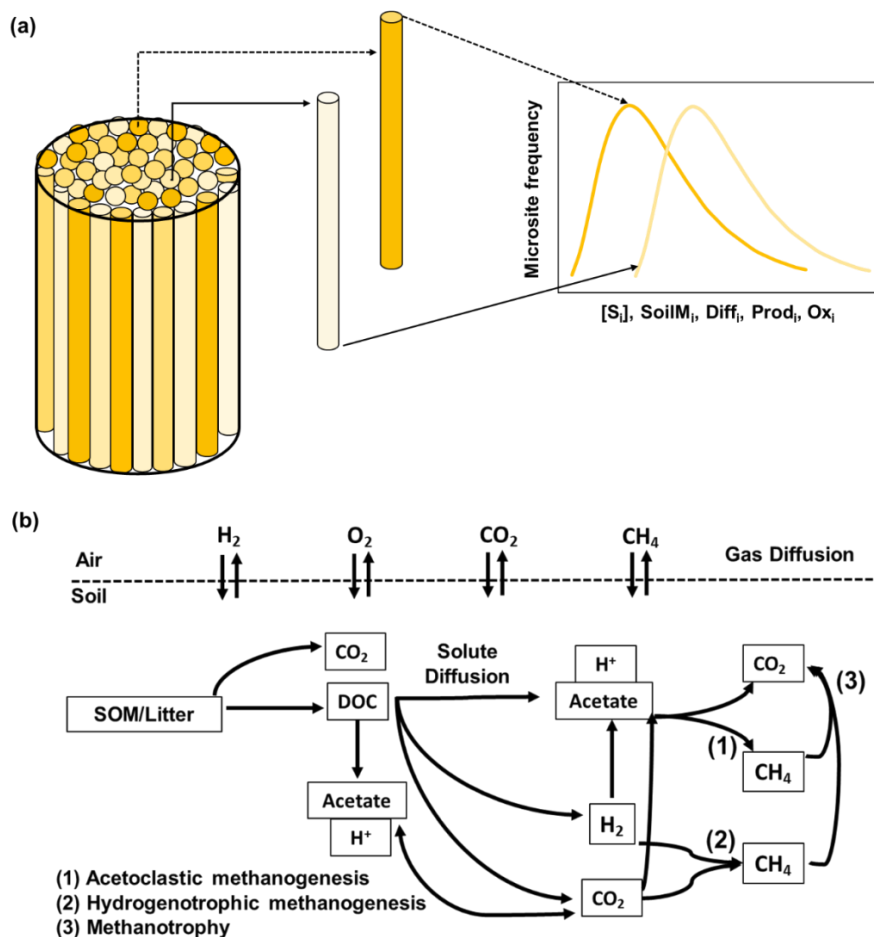
Figure 1: Conceptual figure of the modelling approach. Top panel (a) shows the model representation of soil microsite distribution (modified from Sihi et al., 2020, also see Eq. 13). Different shades indicate substrate concentration [S_i], soil moisture ($SoilM_i$), diffusion ($Diff_i$) of solutes and gases, production ($Prod_i$) and oxidation (Ox_i) processes at each microsite. Bottom panel (b) is the schematic of the microbial functional group-based model coupled with a diffusivity module (Microbial Model for Methane Dynamics-Dual Arrhenius and Michaelis Menten, M3D-DAMM) for simulating soil methane (CH_4) dynamics in field soils (Modified from Xu et al., 2015), where SOM = soil organic matter, CO_2 = carbon dioxide, DOC = dissolved organic carbon, H_+ is the hydronium ion, and H_2 = dihydrogen molecule.
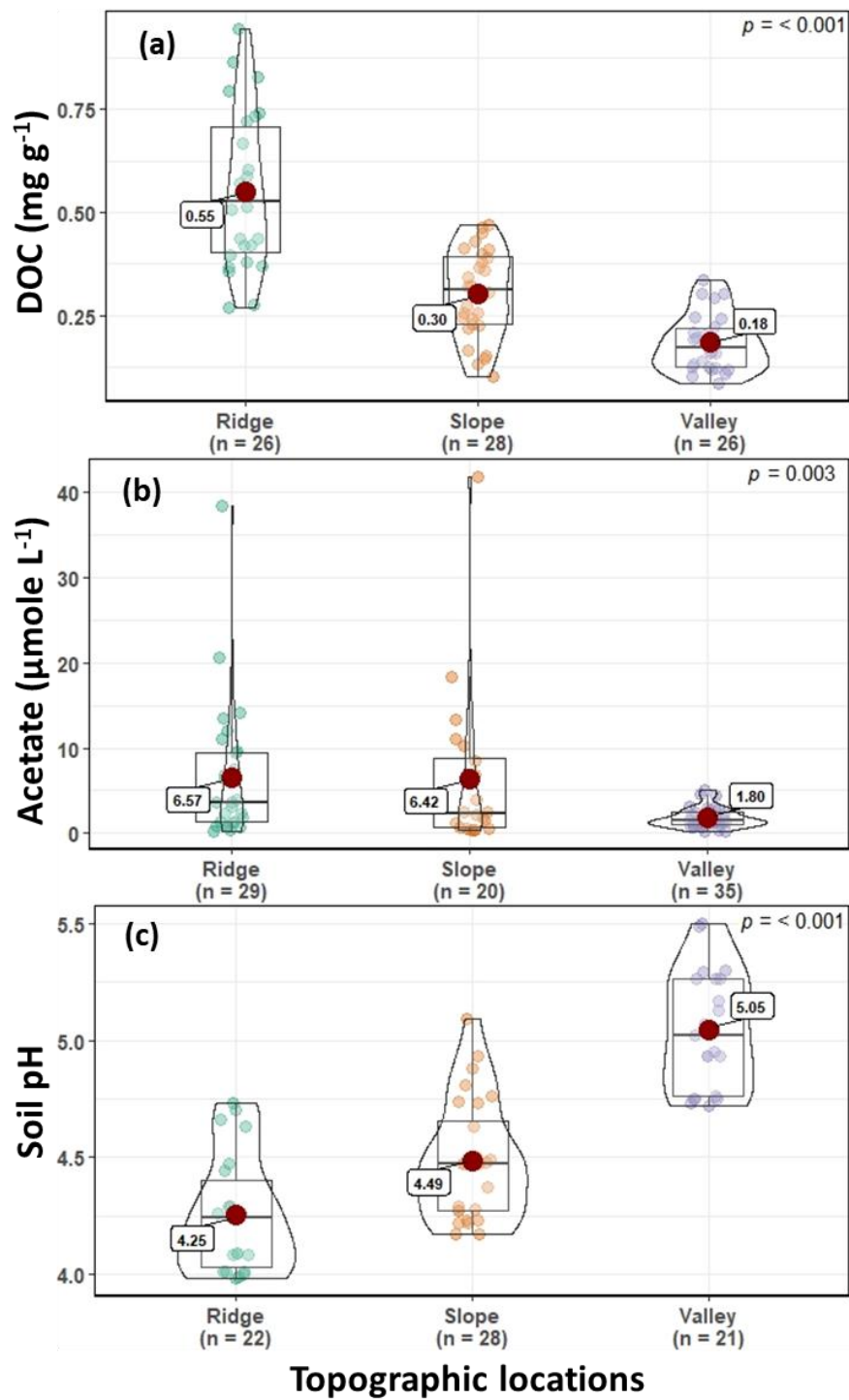
Figure 2: Soil and porewater chemistry (dissolved organic carbon [DOC] (a), acetate (b), and pH (c)) along the ridge-slope-valley topographic gradient.
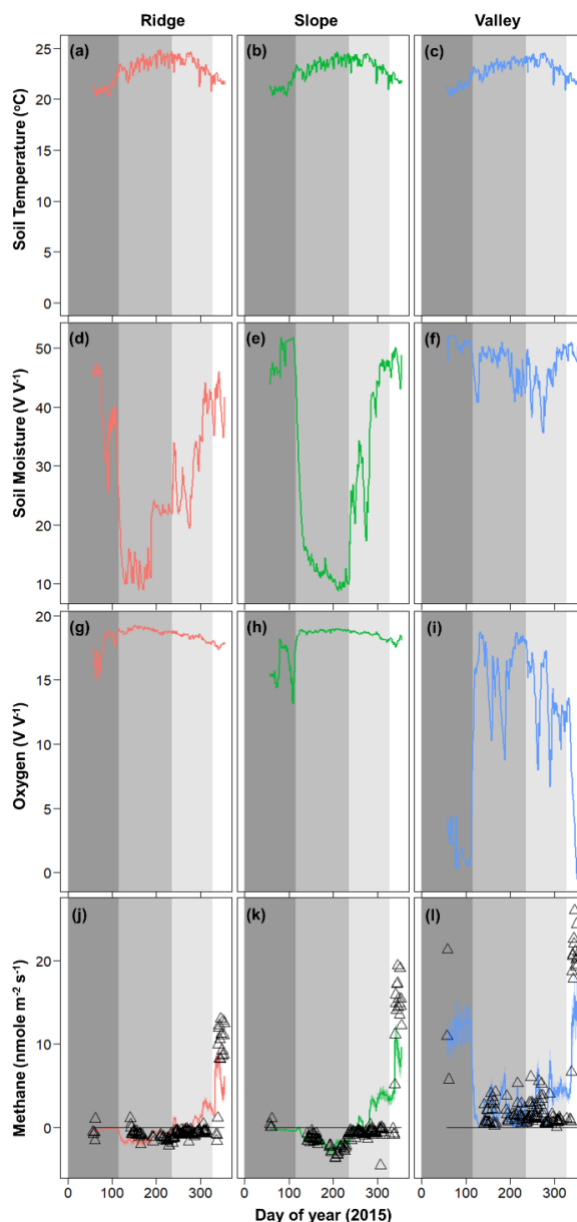
Figure 3: Temporal dynamics of observed meteorological drivers (soil temperature (a-c), soil moisture (d-f), soil oxygen (g-i)) and net methane emissions (j-l) for 2015 (Data are taken from O'Connell et al., 2018). For methane emissions, symbols represent observed data and lines represent model simulations. Dark gray, medium gray, light gray, and white shading represent pre-drought, drought, drought recovery, and post drought events (O'Connell et al., 2018).

23
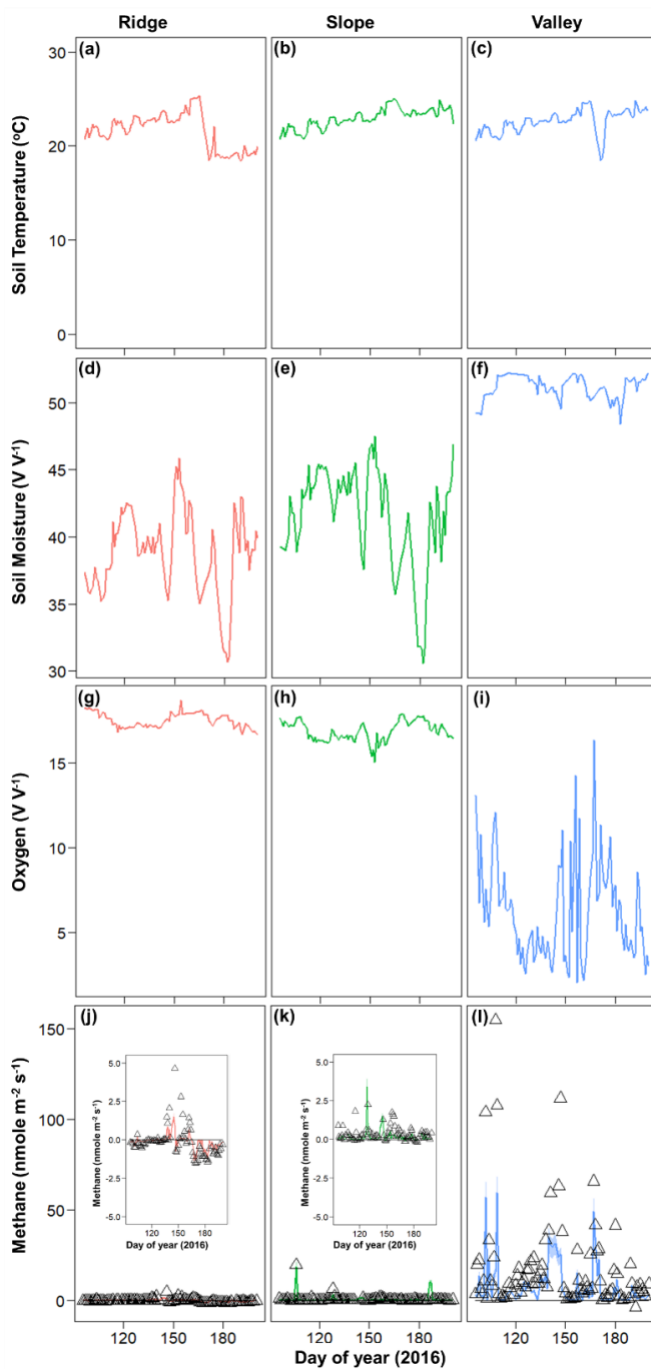
Figure 4: Temporal dynamics of observed meteorological drivers (soil temperature (a-c), soil moisture (d-f), soil oxygen (g-i)) and net methane emissions (j-l) for 2016. For methane emissions, symbols represent observed data and lines represent model simulations.
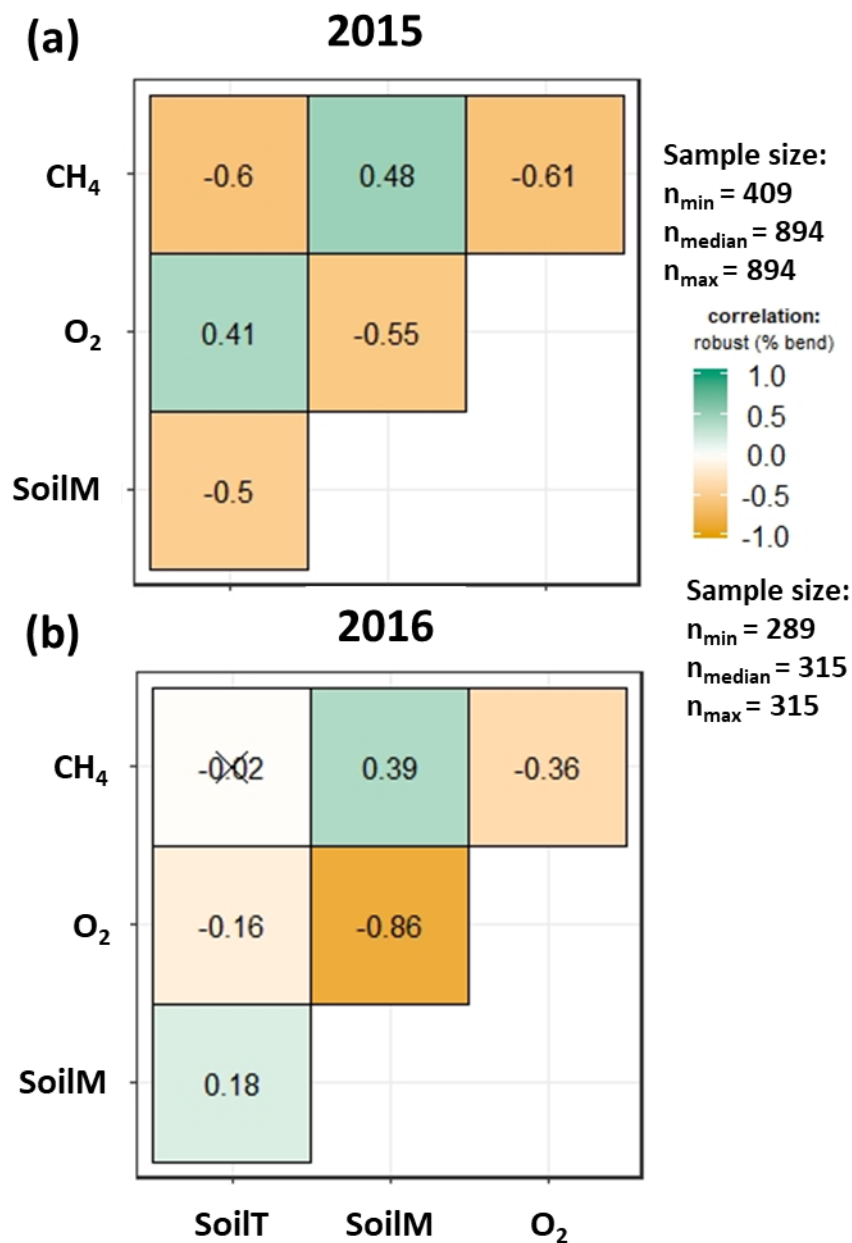
Figure 5: Relation between soil meteorology and methane emissions for 2015 (a) and 2016 (b). SoilM, SoilT, O_2, CH_4 represent soil moisture, soil temperature, oxygen, and methane, respectively. Numbers represent adjusted Holm correlation coefficients, and numbers with "X" indicate a non-significant correlation at $p < 0.05$.
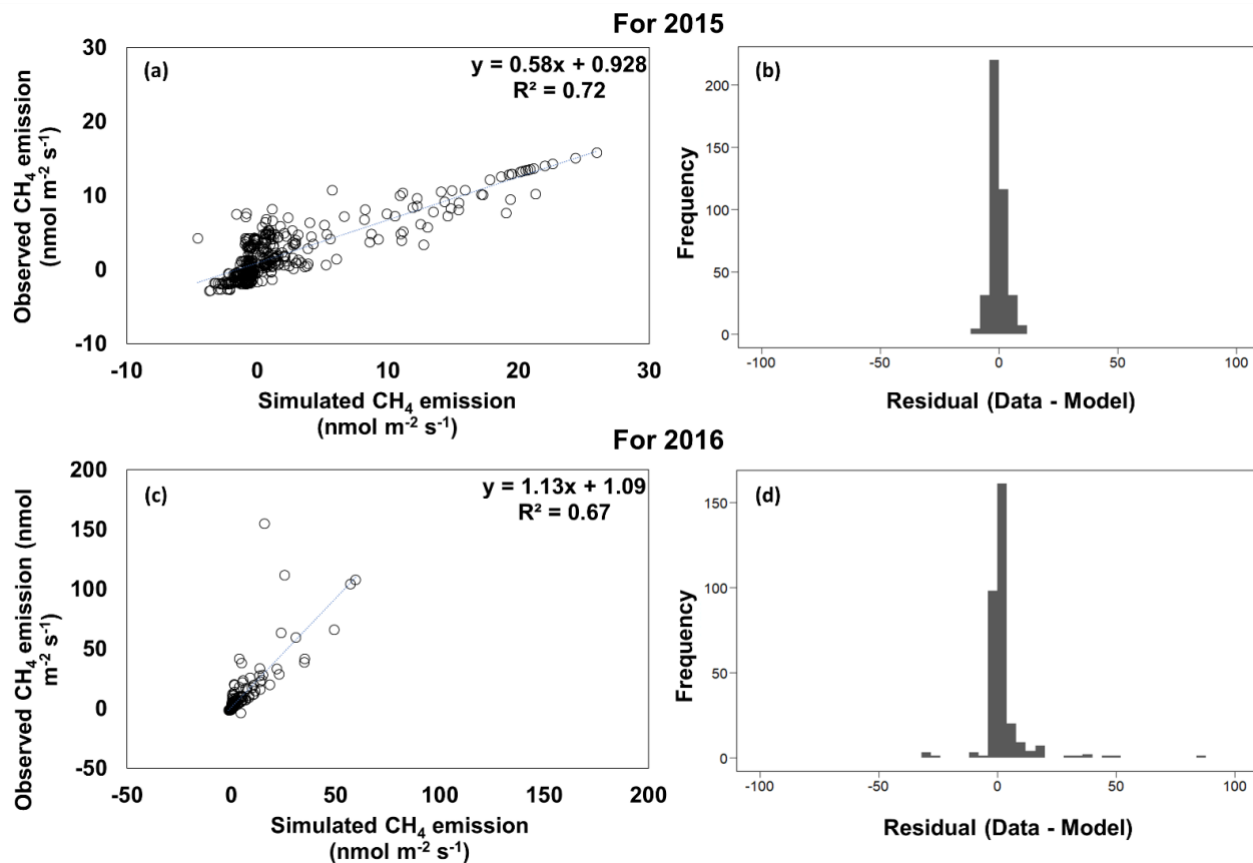
Figure 6: Observed versus simulated methane (CH4) emissions and model residuals for 2015 (a, b) and 2016 (c, d).

690
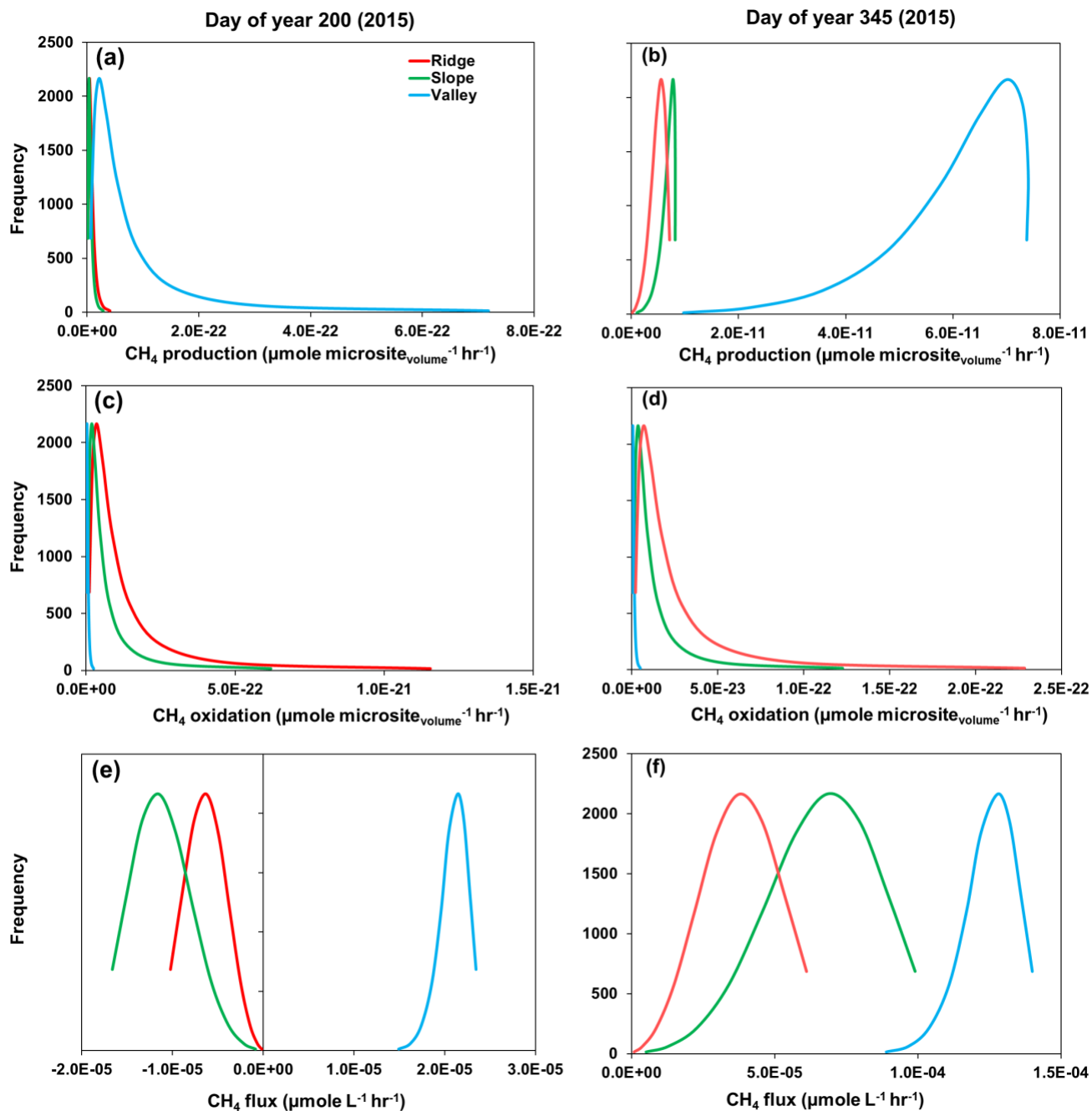
Figure 7: Rates of gross methane (CH4) production (a, b), oxidation (c, d), and net flux (e, f) across simulated soil microsites. Day of year 200 and 345 represent drought and post-drought recovery, respectively (see medium gray and white shading in Fig. 3).

695

Biogeosciences
Discussions
Open Access
EGU
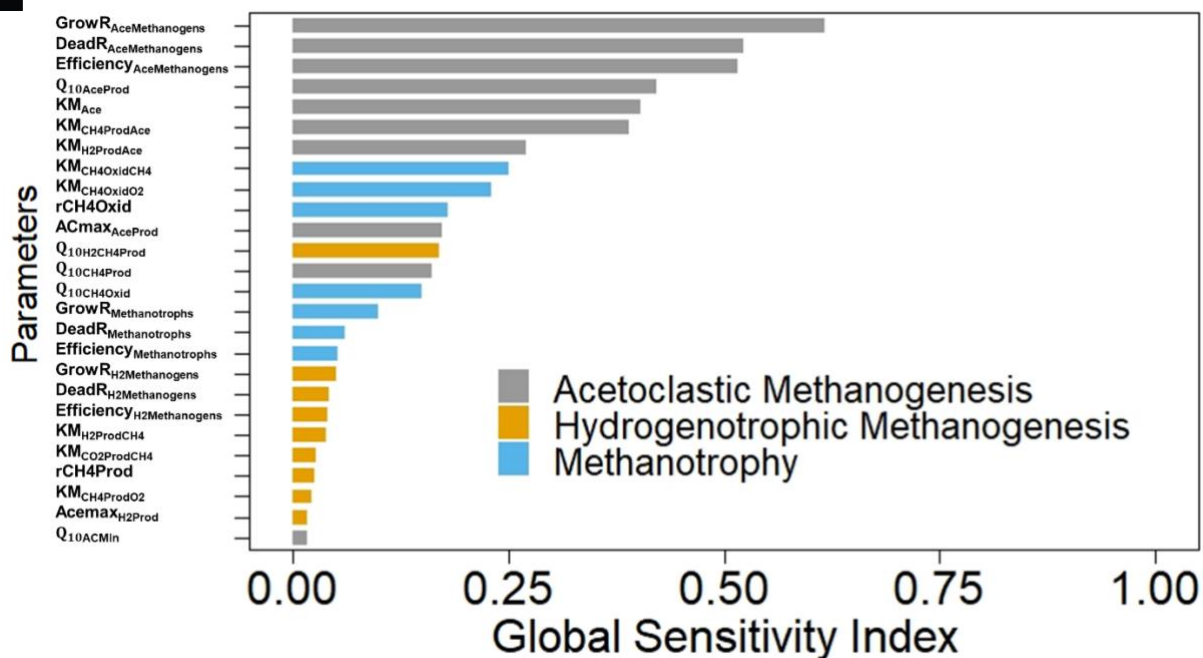
Figure 8: Global sensitivity indices of M3D-DAMM model parameters (defined in Table 1). Gray, yellow, and blue colors represent parameters for acetoclastic methanogenesis, hydrogenotrophic methanogenesis, and methanotrophy, respectively.